

Elsevier Editorial System(tm) for Journal of Hydrology

Manuscript Draft

Manuscript Number: HYDROL6256

Title: A joint model for rainfall-runoff: The case
of Rio Grande Basin

Article Type: Research Paper

Section/Category:

Keywords: Bayesian paradigm

Dynamic Models

Transfer functions

Spatio-Temporal

Spatial change of support

Corresponding Author: Dr Alexandra Mello Schmidt, PhD

Corresponding Author's Institution: Universidade Federal do Rio de Janeiro

First Author: Romy R Ravines, PhD

Order of Authors: Romy R Ravines, PhD; Alexandra M Schmidt, PhD; Helio S Migon, PhD; Camilo D Rennó,
PhD

Manuscript Region of Origin:

Abstract: We present an analysis of runoff and rainfall data from Rio Grande, a basin located in the northeast of Brazil. The main challenges we face here are: (i) to model runoff and rainfall jointly, taking into account their different spatial units, (ii) to use stochastic models where all the parameters have physical interpretations, and (iii) to model

Alexandra Mello Schmidt, PhD
Departamento de Métodos Estatísticos
Instituto de Matemática
Universidade Federal do Rio de Janeiro
Caixa Postal 68530 CEP.: 21945-970
Rio de Janeiro – R.J.
Email: alex@im.ufrj.br
Homepage: www.dme.ufrj.br/alex

Professor R. Krzysztofowicz

University of Virginia
151 Engineer's Way
PO Box 400747
Charlottesville, VA 22904-474 USA

Rio de Janeiro, July, 10th, 2007.

Dear Professor Krzysztofowicz,

Find attached the manuscript entitled "A joint model for rainfall-runoff: The case of Rio Grande Basin" by R. R. Ravines, A. M. Schmidt, H. S. Migon and C. D. Rennó.

We believe this manuscript is within the scope of Journal of Hydrology and are submitting it for publication in the Journal.

I hope to hear from you soon and would like to thank you in advance for your attention.

Yours sincerely,

Alexandra M. Schmidt, Ph.D.

A joint model for rainfall-runoff: The case of Rio Grande Basin

Romy R. Ravines^a Alexandra M. Schmidt^{a,*} Helio S. Migon^a

Camilo D. Rennó^b

^a*Instituto de Matemática, Universidade Federal do Rio de Janeiro, Rio de Janeiro,*

RJ, 21945-970, Brazil

^b*Coordenação Geral de Observação da Terra, Divisão de Processamento de
Imagens, Instituto Nacional de Pesquisas Espaciais, São José dos Campos, SP,*

12227-010, Brazil

Abstract

We present an analysis of runoff and rainfall data from Rio Grande, a basin located in the northeast of Brazil. The main challenges we face here are: (i) to model runoff and rainfall jointly, taking into account their different spatial units, (ii) to use stochastic models where all the parameters have physical interpretations, and (iii) to model these processes in their original scale, without assuming any transformation to attain normality of these variables.

The intrinsically uncertain nature of these hydrological processes makes Bayesian analysis natural in this field. Our approach is based on dynamic models. The effect of rainfall on runoff is modeled through a transfer function, whereas the amount of

rainfall is obtained after fitting a spatio-temporal model and dealing with the change of support problem. Besides the computational effort to implement the proposed models, some methodological novelties are also implemented.

The data consist of monthly series from January 1984 to September 2004, at a runoff station and nine rainfall stations irregularly located in a drainage area of 37522.48 km^2 . Model assessment, spatial interpolation and temporal predictions were part of our analysis. The results show that our approach is a promising tool for rainfall-runoff analysis.

Key words: Bayesian paradigm, Dynamic Models, Transfer functions, Spatio-Temporal, Spatial change of support.

1 Introduction

1 One of the challenges that hydrologists and operators of water resource systems
2 face is to predict the runoff given the rainfall. The intrinsically uncertain nature of
3 these hydrological processes makes Bayesian analysis natural in this field, whenever
4 statistical problems are considered (Rios-Insua et al., 2002).

* *Address for correspondence:* Alexandra M. Schmidt, Departamento de Métodos Estatísticos, Universidade Federal do Rio de Janeiro, Caixa Postal 68530, Rio de Janeiro, RJ, Brazil. CEP 21945-970. *Tel.:* 0055 21 2562-7505 x 204. *Fax:* 0055 21 2562-7374.

E-mail: alex@im.ufrj.br. *Homepage:* www.dme.ufrj.br/~alex

Email addresses: romy@dme.ufrj.br (Romy R. Ravines), migon@im.ufrj.br (Helio S. Migon), camilo@dpi.inpe.br (Camilo D. Rennó).

5 In this paper we present an alternative strategy for dealing with the spatial and
6 temporal features of two of the most important hydrological variables: runoff and
7 rainfall. Our goals are: (i) to model both variables jointly, taking into account their
8 different spatial units, (ii) to use stochastic models where all the parameters have
9 physical interpretations, and (iii) to model these processes in their original scale,
10 without assuming any transformation to attain normality of these variables.

11 Several types of stochastic models have been proposed for the rainfall-runoff rela-
12 tionship, based on deterministic models or on classical time series analysis. Two
13 important classes of stochastic models applied to river flow analysis are: transfer
14 function and regime switching. Transfer function modeling is flexible and has been
15 mainly used in the form of ARMAX models (see, for example, [Sales \(1989\)](#) and
16 [Capkun et al. \(2001\)](#)). Markov Switching time series models, as in [Lu & Berliner](#)
17 [\(1999\)](#) have been recently introduced. These approaches are not ideal, because data
18 transformation is needed and the parameters do not have interpretation in physical
19 terms. Also, in all the previous proposed models, the measurement errors and un-
20 certainty associated with rainfall are not explicitly accounted for. This is because
21 models must describe the rainfall-runoff process on a drainage catchment area ba-
22 sis. However, in practice, precipitation is measured at more than one monitoring
23 station within a basin, thus some procedure is needed in order to approximate the
24 precipitation for the whole basin. There are some widely used methods that make
25 use of polygons to determine the influence area of each station. The total basin's
26 precipitation is computed as a weighted mean of the precipitation measured at each

27 station. The problem with this kind of procedure is that the uncertainty of this
28 estimation is not taken into account when modeling runoff as a function of rainfall.

29 Here we propose a joint model for both variables: rainfall and runoff. For rainfall,
30 we use spatio-temporal models, like in [Sansó & Guenni \(2000\)](#). For runoff, we use
31 non-normal and non-linear Bayesian dynamic models. In particular, we extend the
32 models presented by [Migon & Monteiro \(1997\)](#). Additionally, to approximate the
33 basin's rainfall, we solve the implicit change of support problem (see [Cressie \(1993\)](#)
34 and [Gelfand et al. \(2001\)](#) for further details). The models presented here allow us
35 to represent parsimoniously a complex system of physical processes, which fit and
36 forecast rather well, without losing the physical interpretation of their parameters.

37 Inference procedure is performed under the Bayesian paradigm. Markov Chain Monte
38 Carlo (MCMC) methods are used to assess posterior distributions of the unknown
39 quantities. Since the proposed models can be computationally intensive when fitted
40 with MCMC techniques, we sought to use algorithms that perform thousands of
41 iterations in a few minutes. In particular we focused in the runoff model, for which
42 we used a sampling scheme recently proposed by [Ravines et al. \(2007\)](#). It combines
43 the conjugate updating of [West et al. \(1985\)](#) for dynamic models in the exponential
44 family, with the backward sampling of [Frühwirth-Schnater \(1994\)](#).

45 This paper is organized as follows. In Section 2 we briefly describe the Brazilian data
46 we used to illustrate our methodology. Section 3 is devoted to a general discussion
47 of some particular individual models for runoff and rainfall previously proposed. In

48 Section 4 the joint model proposed here is described and the main aspects of the
49 inference procedure are discussed. In Section 5 we present the results of the analysis
50 of the Rio Grande basin data, and in Section 6 we offer some concluding remarks.

51 **2 Rio Grande Basin, Brazil: Runoff-Rainfall Data**

52 The Rio Grande basin is located in the northeast of Brazil, in Bahia State, a dry
53 sub-humid area with tropical weather. The region under study is between the 11°
54 and 13° South parallels and 43°30' and 46°30' West meridians. This basin has a
55 drainage area of 37522.48 km^2 . The available dataset consists of monthly recorded
56 series from August 1984 to September 2004 (242 months), at one runoff station
57 (Taguá), and nine rainfall stations irregularly located in the drainage area. Figure
58 1(a) shows the location of each station and Figure 1(b) shows the data for the four
59 monitoring stations marked in 1(a).

60 From Figure 1(b) we observe that there are distinct wet and dry periods annually:
61 the rainy season begins in November and lasts through March, with the average
62 accumulated monthly rainfall over 275mm; while the dry season is from late April
63 until October, when the average monthly rainfall rarely exceeds 10mm. Most of the
64 basin is sparsely vegetated and relatively flat, meaning that altitude has no influence
65 in the hydrological regime. Thus, it is not taken into account in our models.

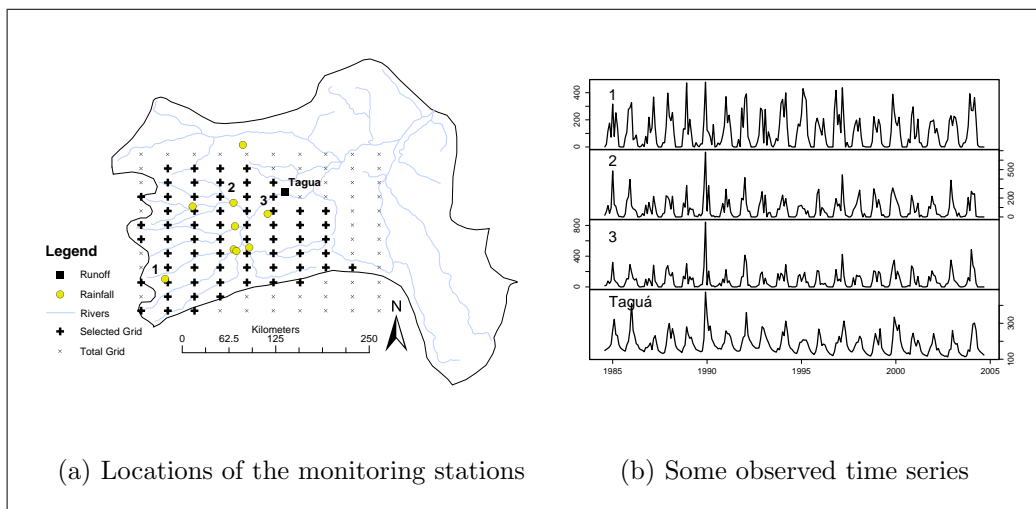


Figure 1. Rio Grande Basin: (a) Locations of the monitoring stations; (b) Time series of monthly runoff at Taguá, and rainfall at sites 1, 2, and 3 (marked in (a)).

66 3 Individual models for rainfall and runoff

67 Two of the main features of the rainfall-runoff relationship are: it is basically non-
 68 linear and the current runoff depends on previous runoff plus current and past
 69 precipitation. It can be assumed that there is no feedback between runoff and rainfall,
 70 so a transfer function model seems to be a natural option for fitting and forecasting
 71 this phenomenon. Besides, runoff is a non-negative variable and its time series can
 72 be non-stationary. Thus, we propose the use of non-linear and non-normal dynamic
 73 models to handle this kind of data.

Let Y_t be the runoff and X_t be the precipitation at time t . The rainfall-runoff rela-

tionship can be represented by

$$Y_t \sim p(Y_t|\mu_t, \phi_t), \quad t = 1, 2, \dots \quad (1a)$$

$$g(\mu_t) = f_1(\alpha_t, E_t) \quad (1b)$$

$$E_t = f_2(E_{t-1}, \dots, E_0, X_t), \quad (1c)$$

74 where $p(Y_t|\mu_t, \phi_t)$ is a density function for a non-negative random variable; μ_t is
 75 the expected value of Y_t ; ϕ_t represents other parameters of $p(Y_t|\mu_t, \phi_t)$; α_t is a basic
 76 level and E_t is the total effect of rainfall at time t ; and $g(\cdot)$, $f_1(\cdot)$ and $f_2(\cdot)$ are
 77 known functions describing the dynamics of the hydrological process. Time varying
 78 parameters and stochastic variations affecting E_t are particular cases of (1).

79 3.1 A dynamic transfer function model

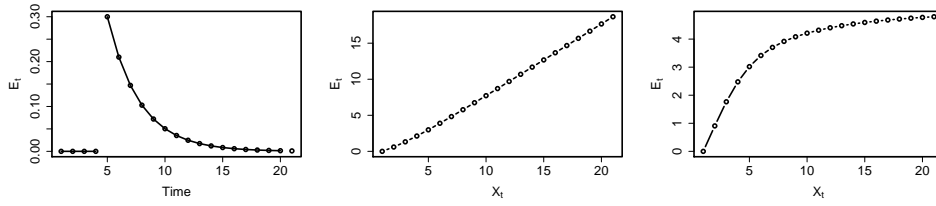
Following the assumptions made in Migon & Monteiro (1997), the relationship between runoff and rainfall can be expressed as a transfer function model. The model in (1) assumes that the expected value of the total runoff generated (streamflow), μ_t , or a function of it, say $g(\mu_t)$, can be written as a baseflow α_t , which depends on the water table level, plus an effect of current and past precipitation E_t , which is $\mu_t = \alpha_t + E_t$. The effect of precipitation is expected to decay between time $t - 1$ and t by a rate $\rho_t \in (0, 1)$. This parameter plays the role of a recharge or rainfall effect memory rate and depends on the geomorphology and land-use/land-cover of the basin. Therefore, it should be (almost) constant over time. Temporal changes in this parameter can be explained by drastic changes in, e.g., soil and/or vegetation char-

acteristics. Since E_{t-1} represents the effect of precipitation before time t , a fraction of current rainfall, say $\gamma_t X_t$, can be added to compute the rainfall effect at time t . The parameter γ_t measures the instantaneous effect of rainfall and is mainly associated with overland flow speed. This parameter has a particular temporal dynamic: it is strongly related to the soil infiltration capacity and the rainfall interception by the vegetation. After a rainy period, the soil is saturated and the overland flow will be high. However, after a dry period, the soil absorbs a great part of water and the overland flow will decrease. Also, when vegetation grows, the leaf density becomes high, increasing the rainfall interception and consequently decreasing its instantaneous effect on the discharge. Alternatively, if ϑ_t is the maximum expected precipitation effect, then $\vartheta_t > \mu_t$ and the remaining possible runoff is $\vartheta_t - (\alpha_t + \rho E_{t-1})$. Therefore E_t , in (1c), can be expressed as one of the following expressions:

$$E_t = \rho_t E_{t-1} + \gamma_t X_t \quad (2a)$$

$$E_t = \rho_t E_{t-1} + [1 - \exp(-\kappa_t X_t)][\vartheta_t - (\alpha_t + \rho_t E_{t-1})]. \quad (2b)$$

80 Equations (2a) and (2b) support the hypothesis that the precipitation effect decays
 81 exponentially with time. In equation (2a), the greater the amount of rainfall, the
 82 greater is its returns to runoff. This hypothesis is known as proportional returns.
 83 On the other hand, in equation (2b), the greater the amount of rainfall, the smaller
 84 is its effect and, moreover, this effect has an upper limit. The latter is known as the
 85 diminishing returns hypothesis. Figure 2 illustrates these functions for some fixed
 86 values of their parameters.



(a) Exponential decay (b) Proportional returns (c) Diminishing returns

Figure 2. Examples of the shapes of the transfer functions in (2a) and (2b).

87 3.2 Modeling rainfall

88 Note that the input X_t in model (1) corresponds to the precipitation of a whole
 89 basin, that is, a unique measure of rainfall is needed at each time t . However, in
 90 many situations, precipitation is observed in more than one station within a basin.
 91 So, the total rainfall for time t , X_t , should be obtained from the solution of the
 92 spatial change of support problem. The change of support problem is concerned
 93 with inference about the values of the variable over areal units (block data) different
 94 from those at which it has been observed (Gelfand et al., 2001). Areal rainfall can
 95 be viewed as a sum over point rainfall data, because it is a continuous univariate
 96 spatial process.

Let $\{X_t(s), s \in B \subset \mathbb{R}^2, t = 1, 2, \dots\}$ be a spatial random field at discrete time t .
 Here, $X_t(s) \geq 0$ is a random variable that represents the amount of rainfall at time
 t and location s . So, the rainfall for a given basin or region B , X_t , is given by

$$X_t = \int_B X_t(s) ds, \quad (3)$$

where B is the basin's domain. In particular, we assume $X_t(s)$ follows a truncated

normal distribution and, as suggested by [Sansó & Guenni \(2000\)](#), is represented by the following spatio-temporal model:

$$X_t(s) = \begin{cases} w_t(s)^\beta & \text{if } w_t(s) > 0, \\ 0 & \text{if } w_t(s) \leq 0 \end{cases} \quad s \in B, \quad (4a)$$

$$\mathbf{w}_t = \mathbf{Z}_t + \boldsymbol{\nu}_t \quad \boldsymbol{\nu}_t \sim GP(\mathbf{0}, \tau^2 \mathbf{I}), \quad (4b)$$

$$\mathbf{Z}_t = \mathbf{F}'\boldsymbol{\theta}_t + \boldsymbol{\epsilon}_t \quad \boldsymbol{\epsilon}_t \sim GP(\mathbf{0}, \sigma^2 \mathbf{V}), \quad (4c)$$

$$\boldsymbol{\theta}_t = \mathbf{G}\boldsymbol{\theta}_{t-1} + \boldsymbol{\omega}_t \quad \boldsymbol{\omega}_t \sim GP(\mathbf{0}, \mathbf{W}_t), \quad (4d)$$

97 where GP denotes a Gaussian process and $\tau^2 \mathbf{I}$ and $\sigma^2 \mathbf{V}$ are the covariance matrices
 98 of \mathbf{w}_t and \mathbf{Z}_t , respectively. Here \mathbf{I} denotes the identity matrix. The term $\boldsymbol{\nu}_t$ is a
 99 random error whose variance, τ^2 , is known as the nugget effect ([Cressie, 1993](#)). The
 100 variance of each $Z_t(\cdot)$ is denoted by σ^2 , and its correlation function is represented by
 101 $\varrho(\|s_i - s_j\|, \lambda) = V_{ij}$, which depends on λ , and on the Euclidean distance, $\|s_i - s_j\|$,
 102 between the locations s_i and s_j . In this case, $\mathbf{F}'\boldsymbol{\theta}_t$ represents a polynomial trend
 103 and \mathbf{G} is the evolution matrix of the parameters $\boldsymbol{\theta}_t$. An alternative way of modeling
 104 rainfall is to use a model derived from a mixture taking into account the excess of
 105 zeros (dry season), as in [Velarde et al. \(2004\)](#) and [Fernandes et al. \(2007\)](#) .

106 Fitting Equations (1) and (3) jointly is our proposed approach. Our formulation
 107 covers a wide class of relationships. It is very flexible and all of its parameters have
 108 a clear interpretation. Moreover, all the uncertainty involved in the physical process
 109 is clearly taken into account, as rainfall is not considered as a known quantity.

110 **4 A simultaneous model for rainfall-runoff**

Assume that we have runoff data from T time periods and rainfall data from S locations over a basin B , observed during the same time period. Let Y_t and X_t be the basin's runoff and rainfall at time t , respectively. Then, \mathbf{Y} denotes the basin's runoff time series, that is, $\mathbf{Y} = (Y_1, \dots, Y_T)'$, and \mathbf{X} denotes the basin's rainfall time series, that is, $\mathbf{X} = (X_1, \dots, X_T)'$. Let $X_t(s_i)$ denotes rainfall at time t and gauged location s_i . Then, $\mathbf{X}_t(\mathbf{s}) = (X_t(s_1), \dots, X_t(s_S))'$ is the rainfall observed at time t over the S gauged locations (for each time t), and $\mathbf{X}(s_i) = (X_1(s_i), \dots, X_T(s_i))'$ is the rainfall time series observed at gauged site s_i (for each location). And, $\mathbf{X}(\mathbf{s}) = (\mathbf{X}(s_1), \dots, \mathbf{X}(s_S))'$, with \mathbf{s} denoting the vector of gauged locations (s_1, \dots, s_S) , is the matrix of rainfall observed at the S locations over T time periods. The joint distribution (see Appendix A for details) of \mathbf{Y} , \mathbf{X} and $\mathbf{X}(\mathbf{s})$ is given by

$$p(\mathbf{Y}, \mathbf{X}, \mathbf{X}(\mathbf{s})|\Theta) = p(\mathbf{Y}|\mathbf{X}, \mathbf{X}(\mathbf{s}), \Theta_Y)p(\mathbf{X}, \mathbf{X}(\mathbf{s})|\Theta_X), \quad (5)$$

111 where $\Theta = (\Theta_Y, \Theta_X)$, Θ_Y denotes the parameters in (1) and Θ_X denotes the
 112 parameters in (4). Note that in (5) the joint distribution of runoff and rainfall
 113 is modeled through the conditional distribution of runoff given rainfall, times the
 114 marginal distribution of rainfall (Schmidt & Gelfand, 2003). Also,

$$\begin{aligned} p(\mathbf{Y}, \mathbf{X}, \mathbf{X}(\mathbf{s})|\Theta) &= \prod_{t=1}^T p(Y_t|X_t, \mathbf{X}_t(\mathbf{s}), \Theta_Y)p(X_t, \mathbf{X}_t(\mathbf{s})|\Theta_X) \\ &= \prod_{t=1}^T p(Y_t|X_t, \mathbf{X}_t(\mathbf{s}), \Theta_Y)p(X_t|\mathbf{X}_t(\mathbf{s}), \Theta_X) \prod_{i=1}^S p(X_t(s_i)|\Theta_X). \end{aligned} \quad (6)$$

115

Gelfand et al. (2001) proposed to approximate $p(X_t, \mathbf{X}_t(\mathbf{s})|\Theta_X)$ by using Monte Carlo integration. They proposed to sample a set of observations in S_B locations, independent and uniformly distributed over B , and compute

$$\hat{X}_t = \sum_{i=1}^{S_B} \hat{X}_t(s_i) \quad i = 1, \dots, S_B, \quad (7)$$

116 where $\hat{X}_t(s_i)$ is the predicted value for rainfall at the i -th location from a regular
 117 interpolation grid (with locations $s_1^*, s_2^*, \dots, s_{S_B}^*$) of S_B points constructed inside the
 118 bounds of B . Consequently, (7) is a Monte Carlo approximation of (3).

The predictive distribution needed for the spatial interpolation of $X_t(s_i)$, at a new set of locations, for instance, $(X_t(s_1^*), \dots, X_t(s_{S_B}^*))'$, is given by

$$p(\mathbf{X}(s')|\mathbf{X}(s)) = \int p(\mathbf{X}(s')|\mathbf{X}(s), \Theta_X)p(\Theta_X|\mathbf{X}(s))p(\Theta_X)d\Theta_X, \quad (8)$$

119 where Θ_X denotes all the parameters in (4).

120 Following the Bayesian paradigm, model specification is complete after assigning
 121 the prior distribution of all the unknowns. From Bayes' theorem we obtain the
 122 kernel of the posterior distribution, which does not have an analytical closed form.
 123 Samples from the posterior distribution can be obtained via Markov chain Monte
 124 Carlo (MCMC) methods (Gelman & Lopes, 2006). Based on the expressions
 125 above, the inference procedure via MCMC can be done in the following steps:

- 126 (1). Fit a spatio-temporal model for rainfall, $\mathbf{X}(\mathbf{s})$, observed at S gauged locations
 127 over B ;
- 128 (2). Build a regular grid over the domain and obtain a sample of the rainfall over

129 the basin, \mathbf{X} , following equations (7) and (8). That is, first obtain a sample
130 from the predictive distribution of $\mathbf{X}(\mathbf{s})$ (for each point of the interpolation
131 grid), then use these values to approximate the rainfall over the basin using
132 equation (7);
133 (3). For each sampled value of rainfall over the basin, X_t , obtained in the previous
134 step, fit the runoff model as in equation (1).

135 In particular, we assume that runoff follows either a lognormal or a gamma distribu-
136 tion. In the case of the lognormal distribution, we applied a log transformation and
137 the algorithm forward filtering backward sampling (FFBS) of [Frühwirth-Schnater](#)
138 [\(1994\)](#) was used to obtain samples of the posterior distribution of interest. In the
139 case of the gamma distribution, we propose the use of a sampling scheme which
140 combines the conjugate updating of [West et al. \(1985\)](#) for dynamic models in the
141 exponential family, with the backward sampling of [Frühwirth-Schnater \(1994\)](#). This
142 algorithm is called conjugate updating backward sampling (CUBS); details are found
143 in [Ravines et al. \(2007\)](#). We note that in non-normal transfer function models CUBS
144 significantly reduces the computing time needed to attain convergence of the chains,
145 and is also very simple to implement.

146 5 Modeling in practice: Inference procedure

We applied the approach described in Section 3 to the rainfall data from the nine stations and the runoff series observed at Taguá station in the Rio Grande basin.

Specifically, we used the function in (2a) for E_t in (1c) and a multivariate dynamic linear model (see [West & Harrison \(1997, Chapter 16\)](#)) for the temporal evolution of the parameters in (4). For a better explanation, we reproduce our whole, general, model in (9).

$$Y_t|X_t \sim p(\mu_t, \phi) \quad t = 1, \dots, T \quad (9a)$$

$$\log(\mu_t) = \alpha_t + E_t \quad (9b)$$

$$E_t = \rho E_{t-1} + \gamma_t X_t + w_t \quad w_t \sim N(0, \sigma_E^2) \quad (9c)$$

$$\alpha_t = \mathbf{G}_\alpha \alpha_{t-1} + w_{\alpha,t} \quad w_{\alpha,t} \sim N(0, \sigma_\alpha^2) \quad (9d)$$

$$\gamma_t = \mathbf{G}_\gamma \gamma_{t-1} + w_{\gamma,t} \quad w_{\gamma,t} \sim N(0, \sigma_\gamma^2) \quad (9e)$$

$$X_t = \sum_{j=1}^{S_B} \hat{X}_t(s_j) \quad j = 1, \dots, S_B \quad (9f)$$

$$X_t(s_i) = \begin{cases} w_t(s_i)^\beta & \text{se } w_t(s_i) > 0 \\ 0 & \text{se } w_t(s_i) \leq 0 \end{cases} \quad i = 1, \dots, S \quad (9g)$$

$$\mathbf{w}_t = \mathbf{z}_t + \boldsymbol{\nu}_t \quad \boldsymbol{\nu}_t \sim N_S(\mathbf{0}, \tau^2 \mathbf{I}) \quad (9h)$$

$$\mathbf{z}_t = \mathbf{F}' \boldsymbol{\theta}_t + \boldsymbol{\epsilon}_t \quad \boldsymbol{\epsilon}_t \sim N_S(\mathbf{0}, \sigma^2 \mathbf{V}_t) \quad (9i)$$

$$\boldsymbol{\theta}_t = \mathbf{G} \boldsymbol{\theta}_{t-1} + \boldsymbol{\epsilon}_t \quad \boldsymbol{\epsilon}_t \sim N_k(\mathbf{0}, \mathbf{W}_t) \quad (9j)$$

$$\boldsymbol{\theta}_0 \sim N(\mathbf{0}, \mathbf{100I}), \quad (9k)$$

147 where $p(\mu_t, \phi)$ is the log-normal or gamma distribution and ϕ corresponds to the
 148 precision parameter of the former and the shape parameter of the latter. In (9g)–
 149 (9k), S is the number of monitoring sites and S_B is the number of points in the
 150 interpolation grid. $X_t(s_i)$ denotes the rainfall at time $t = 1, \dots, T$ and site $s_i =$

151 s_1, \dots, s_S , $w_t(s_i)$ is a latent Gaussian variable, β is an unknown power, \mathbf{w}_t is a vector
 152 of dimension S that stacks the S observations made at time t , τ^2 is a nugget effect,
 153 $\sigma^2 > 0$ and \mathbf{V}_t is a spatial correlation matrix of dimension S . Here we assume that
 154 $V_{s_i, s_{i'}} = \exp(-\lambda d_{s_i, s_{i'}})$, that is, an exponential decay correlation where λ controls
 155 the decay rate, $\lambda > 0$ and $d_{s_i, s_{i'}}$ is the Euclidean distance between sites s_i and $s_{i'}$,
 156 $i, i' = 1, \dots, S$. In (9i)–(9k), \mathbf{F}' is an $S \times k$ matrix, \mathbf{G} is a $k \times k$ matrix and $\boldsymbol{\theta}$ is a
 157 vector of dimension k . The elements of $\boldsymbol{\theta}$ are such that $\boldsymbol{\theta}_t = (\boldsymbol{\theta}_{t1}, \boldsymbol{\theta}_{t2})'$, where $\boldsymbol{\theta}_{t1}$ is
 158 a sub-vector that describes the spatial trend and $\boldsymbol{\theta}_{t2}$ describes the seasonal effects.
 159 Equations (9d) and (9e) represent possible time evolutions of α and γ , respectively.
 160 In practice, just one of these equations is considered and depends on the features of
 161 the basin under study.

162 5.1 Prior distributions and full conditional distributions

163 In general, we used fairly vague prior distributions. However, since all the involved
 164 parameters have physical interpretations, an elicitation procedure could be done. For
 165 the parameters of the spatio-temporal model in (9g)–(9k), we set $p(\boldsymbol{\theta}_0, \sigma^2, \zeta^2, \lambda, \beta) =$
 166 $p(\boldsymbol{\theta}_0)p(\sigma^2)p(\zeta^2)p(\lambda)p(\beta)$, where $\zeta^2 = \tau^2/\sigma^2$, $p(\boldsymbol{\theta}_0)$ is an S -variate normal distri-
 167 bution with mean $\mathbf{0}$ and an identity covariance matrix, $N_S(\mathbf{0}, \mathbf{I})$ and $p(\sigma^2)$ is an
 168 improper distribution, $1/\sigma^2$. On the other hand, $p(\zeta^2)$, $p(\lambda)$ and $p(\beta)$ are gamma
 169 densities with parameters $(0.001, 0.001)$, $(2.00, 6/1.86)$ and $(12, 4)$, respectively. The
 170 hyper-parameters for λ were selected according to the premise that at half of the
 171 maximum distance between the observed points, the spatial correlation is almost

172 zero. The hyper-parameters for the prior of β were chosen such that its expected
 173 value was 3, representing the cubic root transformation recommended in the hydro-
 174 logical literature (Sansó & Guenni, 2000).

Following Bayes' Theorem, the posterior distribution is proportional to the likelihood times the prior distribution. For the spatio-temporal model in (9g)-(9k), the posterior distribution is given by

$$\begin{aligned}
 p(\sigma^2, \varsigma^2, \lambda, \beta, \mathbf{z}, \boldsymbol{\theta} | \mathbf{X}) &\propto \left(\frac{1}{\sigma^2}\right)^{ST} \left(\frac{1}{\varsigma^2}\right)^{ST/2} |\mathbf{V}(\lambda)|^{-T/2} \\
 &\exp\left(-\frac{1}{2\sigma^2} \sum_{t=1}^T \frac{1}{\varsigma^2} \|\mathbf{w}_t - \mathbf{z}_t\|^2 + (\mathbf{z}_t - \mathbf{F}'\boldsymbol{\theta}_t)' \mathbf{V}(\lambda)^{-1} (\mathbf{z}_t - \mathbf{F}'\boldsymbol{\theta}_t)\right) \\
 &-\frac{1}{2} \sum_{t=1}^T (\boldsymbol{\theta}_t - \mathbf{G}\boldsymbol{\theta}_{t-1})' \mathbf{W}_t^{-1} (\boldsymbol{\theta}_t - \mathbf{G}\boldsymbol{\theta}_{t-1}) \left(\prod_{x_{it}>0} \frac{x_{it}^{1/\beta-1}}{\beta}\right) p(\boldsymbol{\theta}_0, \sigma^2, \varsigma^2, \lambda, \beta). \quad (10)
 \end{aligned}$$

175 From (10), we have the following full conditional distributions (f.c.d.): σ^2 and ς^2
 176 are inverse gamma, \mathbf{z} is multivariate normal, and $w_{ij} < 0$ is a univariate truncated
 177 normal. The f.c.d. of λ and β do not have a known closed form. Since $\boldsymbol{\theta}_t$ are the
 178 state parameters of a normal dynamic model, their f.c.d. are multivariate normals.

179 For the dynamic models in (9a)-(9c) we also set independent priors to all the para-
 180 meters. In particular, we considered normal prior distributions with zero mean and
 181 variance 10^3 for E_0 , α and γ and a uniform distribution over $[0, 1]$ for ρ . For all the
 182 variance terms, $(\sigma_Y^2, \sigma_E^2, \sigma_W^2)$, we assigned inverse gamma distributions with both
 183 hyper-parameters equal to 0.01. When the gamma distribution is used to model
 184 the runoff, a gamma distribution with both parameters equal to 0.01 was used as a
 185 prior for ϕ , the shape parameter in (9a). In this case, the f.c.d. of the unknowns in
 186 (9a)-(9c) depend on the distribution assumed for Y_t and the hypothesis for $\sigma_E^2, \sigma_\alpha^2$

187 and σ_γ^2 . In particular, if $p(\mu_t, \phi)$ is a gamma distribution and $\sigma_\alpha^2 = \sigma_\gamma^2 = 0$, the f.c.d.
188 of γ and σ_E^2 are normal and inverse gamma, respectively, and the f.c.d. of α , ρ and
189 ϕ do not have a known closed form.

190 5.2 Some computational details

191 In order to sample from the posterior distribution, we used a hybrid Gibbs sam-
192 pling algorithm (Gelfand & Smith, 1990). Samples from the f.c.d. of λ, β, α and ρ
193 were obtained through the slice sampling algorithm (Neal, 2003). We made use of
194 a Metropolis-Hastings step to sample ϕ . Samples from $\boldsymbol{\theta}_t$ were obtained with the
195 forward filtering backward sampling (FFBS) procedure (Frühwirth-Schnater, 1994).
196 Following Sansó & Guenni (2000), we used discount factors for \mathbf{W}_t : $\delta_T = 0.90$ for
197 the spatial trend and $\delta_S = 0.95$ for the seasonal effects. Finally for σ_α^2 and σ_γ^2 we
198 used a discount factor of 0.95, whenever these parameters were considered in the
199 model.

200 The MCMC algorithm for the spatio-temporal model was iterated 70 000 times after
201 a burn-in of 10 000 steps, for two parallel chains. We stored every 10th iteration.
202 For the runoff models we ran two chains for 60 000 iterations, after a burn-in period
203 of size 10 000. The samples were taken at every 5th step. All the algorithms were
204 written in `0x` version 3.20 (see Doornik (2002)). The convergence of our chains was
205 checked with the tests available in the CODA package, developed by Plummer et al.
206 (2005), for the software R version 2.40.

207 *5.3 Results*

208 Taking advantage of the factorization of the likelihood in $p(Y_t|X_t)p(X_t)$, we used
 209 the computational routines for fitting the model in (3) with some different cases of
 210 polynomial trend, and then fitting several particular cases of the model in (1).

211 Our final model for rainfall has an intercept and a linear effect of longitude. Al-
 212 ternative models had shown that latitude has no significant effect in this region.

213 The seasonal pattern was represented via two Fourier harmonics, which were chosen
 214 through an exploratory analysis of the periodogram of the series. Therefore matrix
 215 \mathbf{F}_t in (9i) has row components: $(1, \text{longitude}(s_i), 1, 0, 1, 0)'$ and $\mathbf{G} = \text{diag}(\mathbf{G}_1, \mathbf{G}_2)$,

216 where \mathbf{G}_1 is an identity matrix of order 2, and \mathbf{G}_2 has diagonal blocks

$$217 \mathbf{G}_{2r} = \begin{pmatrix} \cos(2\pi r/12) & \sin(2\pi r/12) \\ -\sin(2\pi r/12) & \cos(2\pi r/12) \end{pmatrix}, r = 1, 2.$$

218 Figure 3 shows the estimated paths of $\boldsymbol{\theta}_t$. We observe that the intercept clearly
 219 varies over time and seems to have an inter-annual cycle. The effect of longitude
 220 is negative and varies smoothly over time. The first harmonic has a very regular
 221 pattern, however the effect of the second harmonic exhibits two periods of different
 222 behaviors: before and after 1992. Table 1 presents the main summaries of the pos-
 223 terior samples obtained for the static parameters in equations (9g)-(9k). Note that
 224 we made inference about $\zeta^2 = \tau^2/\sigma^2$. The posterior mean of β is 1.73, suggesting
 225 that the data is smoothly skewed, probably because we are working with monthly

226 data. In Table 1 we also observe that the \hat{R} statistics (Gelman & Rubin, 1992) take
 227 values close to 1, suggesting that the convergence of our chains was reached.

228 In order to illustrate the fitted values produced by our spatio-temporal model, Figure
 229 4 displays the mean of the predictive posterior distribution of rainfall for two selected
 230 months. Note that different patterns are obtained for a rainy month (like December)
 231 and a dry month (like June).

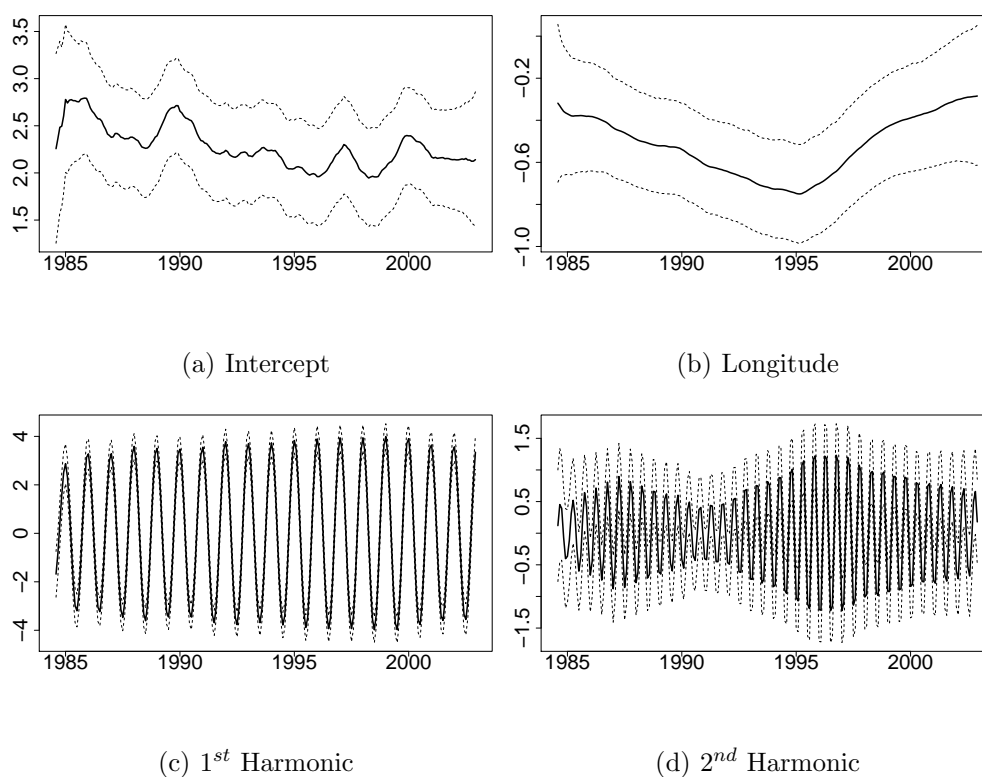


Figure 3. Estimated path of the state parameters for the rainfall model in (9k). Solid lines correspond to the posterior mean and dashed lines to the 95% posterior credible intervals.

232 The basin's rainfall was obtained by means of the spatial interpolations of rainfall
 233 over a grid of 63 points selected from a regular grid constructed over the whole

Table 1

Posterior summaries associated with the parameters in equations (9g)-(9k)

Parameter	mean	sd	2,5%	25%	50%	75%	97,5%	\hat{R}
β	1.732	0.016	1.701	1.722	1.732	1.743	1.764	1.001
λ	0.045	0.007	0.033	0.040	0.044	0.050	0.061	1.001
ζ^2	0.719	0.040	0.644	0.691	0.718	0.746	0.798	1.001
σ^2	1.100	0.044	1.015	1.070	1.098	1.128	1.191	1.003

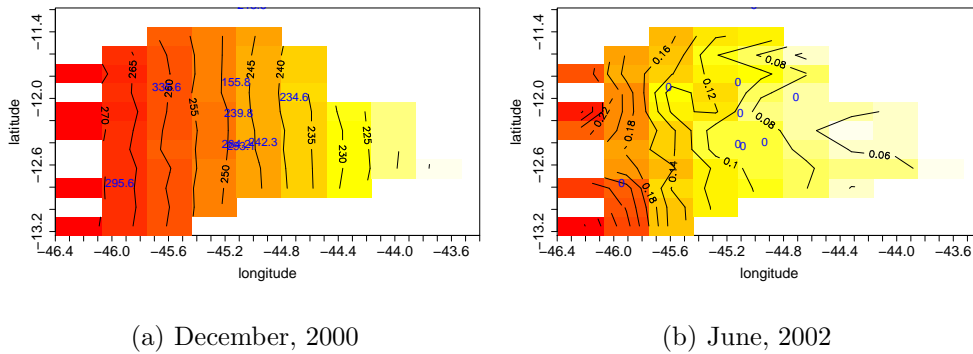
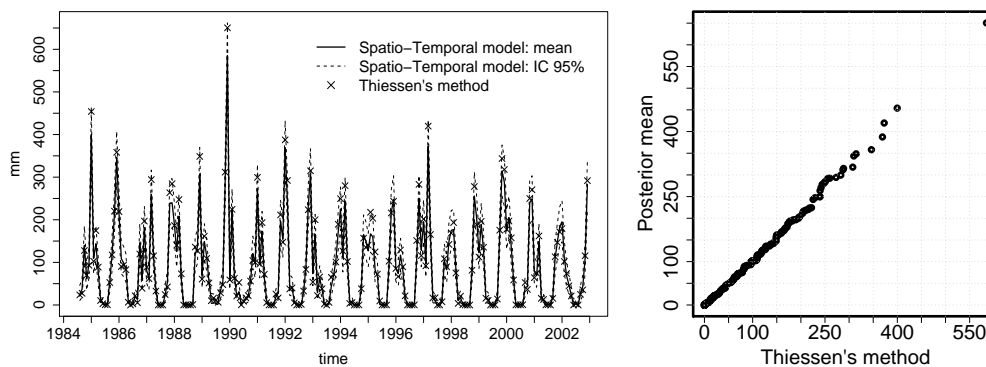


Figure 4. Posterior mean for rainfall for two different months. Dots mark the location of the rainfall monitoring stations. Darker values indicate higher rainfall values.

234 basin under study. This grid is exhibited in Figure 1(a). The integral in (9f) was
 235 approximated by summing the 63 predicted values at each iteration of our MCMC
 236 algorithm. The resulting areal rainfall series, posterior mean and 95% credible inter-
 237 vals are displayed in Figure 5. This figure also shows the mean areal precipitation
 238 estimated by the Thiessen method, a widely used deterministic method. It consists
 239 of assigning an area, or weight, called a Thiessen polygon, to each site. Then the
 240 individual weights are multiplied by the observed station and the values are summed
 241 up to obtain the areal average precipitation. Figure 5 warrants attention because
 242 under the Bayesian framework we take into account the uncertainty involved and



(a) Mean and 95% interval

(b) *Q-Q plot*

Figure 5. Panel (a): Areal rainfall (solid line corresponds to the posterior mean and dashed lines to the 95% credible interval. + corresponds to the Thiessen method estimation). Panel (b): *Q-Q plot* between the estimated rainfall over the basin obtained via the Thiessen's method and the posterior mean of the predictive distribution, as in equation (7).

243 have a credible interval for each time. Therefore, this uncertainty will naturally be
 244 taken into account during the fitting of the runoff part of the model. Notice also that
 245 the estimated rainfall under the Thiessen method seems to be close to the upper
 246 limit of the posterior predictive interval. This suggests an overestimation of rainfall
 247 for some instants in time. This is also clear from the *Q-Q plot* presented on panel
 248 (b) of Figure 5.

249 We used our posterior sample of the basin's rainfall to fit several particular cases
 250 of equations (9a)-(9c). Specifically, for $p(Y_t|X_t)$, we considered the two distribution
 251 mentioned above: log-normal and gamma. We also considered the following five
 252 specifications:

253 (a) The basic level, the transfer function and the instant rainfall effect are static;

254 that is: $\sigma_\alpha^2 = \sigma_\gamma^2 = \sigma_E^2 = 0, \forall t$.

255 (b) The basic level and the instant rainfall effect are static. The transfer function

256 is stochastic: $\sigma_\alpha^2 = \sigma_\gamma^2 = 0$ and $\sigma_E^2 > 0, \forall t$.

257 (c) The basic level follows a random walk. The transfer function and the instantane-

258 nous rainfall effect are static: $\alpha_t = \alpha_{t-1} + w_{\alpha,t}, \sigma_\alpha^2 > 0$ and $\sigma_\gamma^2 = \sigma_E^2 = 0, \forall t$.

259 (d) The basic level is static, the transfer function is stochastic and the instantaneous

260 rainfall effect follows a random walk: $\gamma_t = \gamma_{t-1} + w_{\gamma,t}, \sigma_\gamma^2 > 0, \sigma_\alpha^2 = 0$ and

261 $\sigma_E^2 > 0, \forall t$.

262 (e) The basic level is static, the transfer function is stochastic and the instantaneous

263 rainfall effect varies over time following a constant trend and a seasonal pattern:

264 $\gamma_t = \mathbf{G}_\gamma \gamma_{t-1} + w_{\gamma,t}, \sigma_\gamma^2 > 0, \sigma_\alpha^2 = 0$ and $\sigma_E^2 > 0, \forall t$. $\mathbf{G}_\gamma = \text{diag}(1, \mathbf{G}_{2,\gamma})$, where

$$265 \mathbf{G}_{2,\gamma} = \begin{pmatrix} \cos(2\pi r/12) & \sin(2\pi r/12) \\ -\sin(2\pi r/12) & \cos(2\pi r/12) \end{pmatrix}, r = 1, 2.$$

266 It is worth pointing out that we also fitted the function in (2b), however the results

267 were less satisfactory than those under (2a) in terms of goodness of fit (to this

268 particular dataset). Model comparison was performed using the following criteria:

269 (i) Deviance Information Criterion (DIC), proposed by Spiegelhalter et al. (2001);

270 (ii) Expected Predictive Deviation (EPD), proposed by Gelfand & Ghosh (1998);

271 (iii) Mean Square Errors (MSE); and (iv) Mean Absolute Errors (MAE). In all cases,

272 smaller values indicate the best model among those under study.

273 Table 2 (columns 4, 7, 8 and 9) shows the values of DIC, EPD (both considering

274 a quadratic loss), MSE and MAE, computed for each of the five specifications de-

275 scribed above. Two conclusions can be drawn from this table: first, all the criteria
276 suggest that the gamma distribution should be chosen (this is no longer valid for
277 columns 10 and 11); and second, in this case, specification (e) provides better results
278 in terms of goodness of fit. It is worth mentioning that when using the rainfall time
279 series obtained through the Thiessen's method as input (X_t) in the selected model,
280 the values of DIC and EPD are 1817.6 and 90343, respectively. More specifically, as
281 expected, the penalty term of both criteria is smaller, however the goodness of fit
282 term is poorer. In other words, our joint model produces better results (fitted values)
283 than the individual model that assumes rainfall as known. A similar conclusion is
284 obtained when using just the posterior mean of the areal rainfall obtained from the
285 spatio-temporal model.

286 Our final runoff model, therefore, assumes a gamma distribution with a static basic
287 level, a stochastic transfer function and an instant rainfall effect varying across time
288 following a constant trend and a seasonal pattern. In Figures 6(a) and 6(b) we
289 show the histograms of the samples from the posterior distributions of α and ρ ,
290 respectively. Figure 6(a) shows the posterior mean of α is 4.84, indicating that the
291 mean basic level in that region, during the observed time period, was $126.46 \text{ m}^3/\text{s}$.
292 Figure 6(b) shows that the mean of the regional recharge is 0.64 and varies between
293 0.57 and 0.71, which corresponds to the 95% posterior credible interval. Figure 6(c)
294 shows the evolution of the rainfall's instant effect, $\gamma_t X_t$. Remember that in the
295 selected model, γ_t is a vector with five components where the first one corresponds
296 to the constant trend and the last four correspond to the two harmonics used. Panel

Table 2

Model comparison criteria for three alternative specifications of (9a)-(9c): Deviance Information Criteria (DIC), Expected Predictive Deviance (EPD), Mean Square Error (MSE) and Mean Absolute Error (MAE).

Model	\bar{D}	pd	DIC	Fit	Penalty	EPD	MSE ^a	MAE ^a	MSE ^b	MAE ^b
Log-normal distribution for Runoff (Y_t)										
(a)	1917.6	27.7	1 945.3	103 475	94 948	198 423	429.1	14.9	1 366.9	27.5
(b)	1733.0	99.9	1 833.0	58 577	33 096	91 674	149.9	7.4	1 359.3	26.8
(c)	1799.8	50.0	1 849.9	65 485	64 745	130 231	292.1	10.3	2 058.4	27.5
(d)	1757.5	86.3	1 843.9	62 068	40 870	102 939	186.5	8.4	1 588.6	25.7
(e)	1887.2	120.1	2 007.3	125 683	60 749	186 433	274.2	9.7	1 596.4	26.2
Gamma Distribution for Runoff (Y_t)										
(a)	1917.8	16.8	1 934.6	103 157	94 412	197 570	427.5	14.8	1 398.6	26.5
(b)	1718.6	110.5	1 829.1	55 038	29 476	84 514	134.3	7.0	1 119.6	26.0
(c)	1810.7	27.3	1 838.1	73 879	61 528	135 407	280.2	10.0	2 078.2	28.0
(d)	1722.9	108.6	1 831.6	56 077	30 525	86 602	139.0	7.2	1 434.8	26.8
(e)	1679.5	138.3	1 817.9	50 692	19 764	70 457	88.8	5.6	1 583.0	26.5

^a With fitted values: in the sample, (221 months),

^b With predicted values: out-of-sample. (21 months).

297 6(d) shows the trajectory of the first component of γ_t . In this panel we observe that
 298 the rainfall's instant effect (without the seasonal effects) is always greater than zero
 299 and its value varies between 0.03 and 0.05. We also observe a decreasing trend for
 300 the last months.

301 One of the advantages of the Bayesian approach is that at the end of the inference
 302 procedure we have a sample from the posterior distributions of all the unknowns in
 303 the models. Therefore, it is straightforward to make inferences about functions of

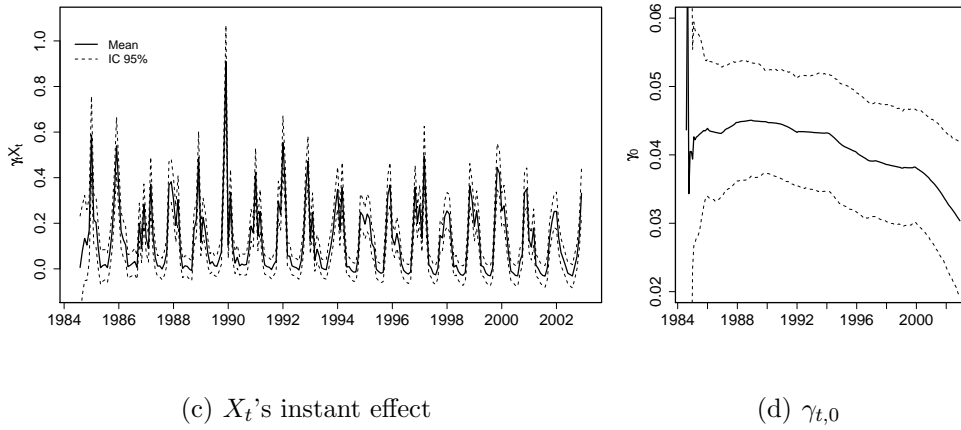
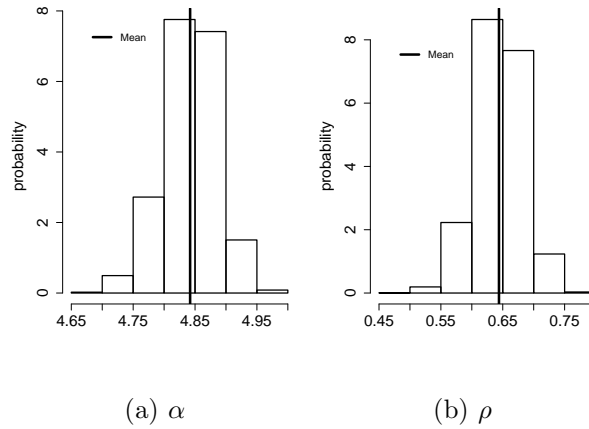


Figure 6. Parameters in (9a)-(9c), with specification (e) and gamma response.

304 these quantities. The impulse-response function is probably one of the most impor-
 305 tant results of the class of models we proposed for runoff. This function indicates
 306 the intensity of the runoff response and how many periods the effect of a impulse
 307 of rainfall persists. Based on the posterior samples of γ and ρ , we constructed the
 308 impulse-response function presented in Figure 7(a). In this case, we considered that
 309 there is no precipitation during 26 months, except at time $t = 5$. In Figure 7(b)
 310 we considered the first values of rainfall as inputs or impulses. In both figures, gray
 311 points correspond to the posterior samples of each function, and dotted lines corre-

312 spond to the 95% posterior credible intervals.

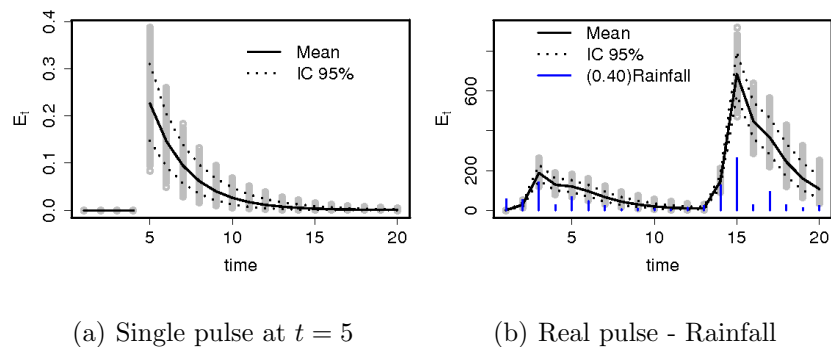


Figure 7. Runoff Impulse-Response Function. Solid line represents the mean and dotted lines represent the 95% posterior credible interval.

313 Figure 8(a) shows the fitted values obtained for the 221 months in the runoff series.
 314 Note that the observed runoff values are within the limits of the 95% interval of the
 315 posterior predictive distribution, indicating an acceptable overall fit. However, it
 316 can be observed that the higher observed values (over $300 \text{ m}^3/\text{s}$) are near the upper
 317 limit, suggesting the use of an extreme value distribution to model them. This lack
 318 of fit at the upper tail is also revealed by the Q-Q plot among observed values and
 319 posterior predictive means displayed in Figure 8(b).

320 5.4 Temporal predictions and spatial interpolations

321 An important issue to be considered here is that fitted and forecast values obtained
 322 from Bayesian rainfall-runoff models can be used in synthetic hydrology. As pointed
 323 out by [Rios-Insua et al. \(2002\)](#), the sample of the predictive distributions can be
 324 used to simulate sequences of observations that mimic some behavior phenomenon
 325 for engineering design or analysis. Therefore, good interpolated and forecast values

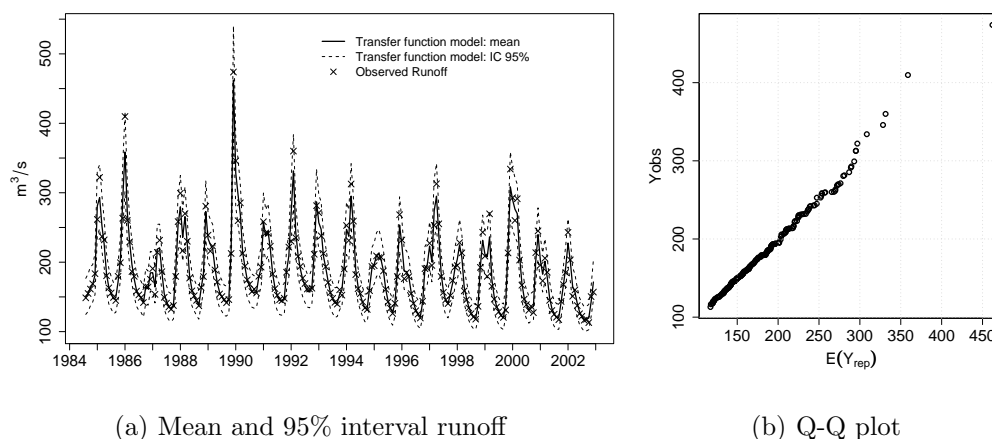


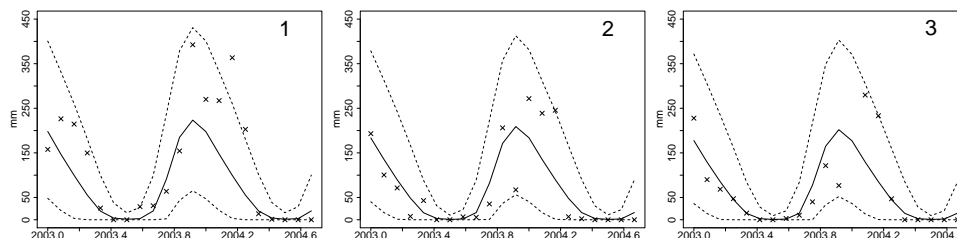
Figure 8. Runoff fitted values, under Model (9a)-(9c). The solid line corresponds to the posterior mean and dashed lines to the limits of the 95% credible interval. + corresponds to observed data.

326 are important to support other areas of hydrological research.

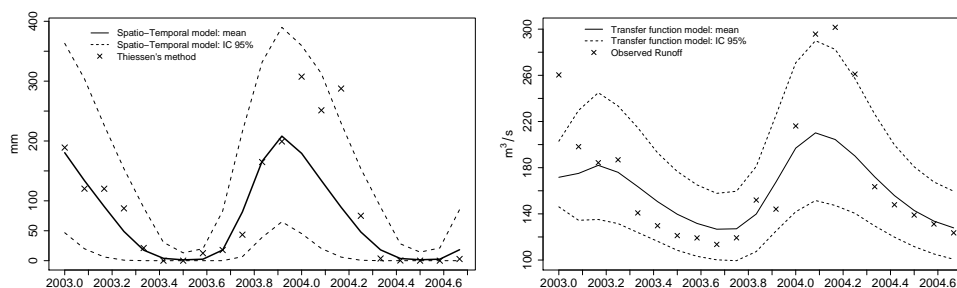
327 In order to evaluate the interpolations and predictions obtained with our models,
 328 we left the last 21 observations out of the sample. The predictive distribution of
 329 rainfall was used to forecast the precipitation at each monitoring station. Also, as
 330 we stated in Section 4, at each iteration of the MCMC algorithm, we used the
 331 predictive distribution of rainfall to compute the areal one and then we forecast the
 332 runoff.

333 From columns 10 and 11 of Table 2, we conclude that the selected model (gamma
 334 distribution and specification (e)) does not exhibit the smallest out-of-sample MSE
 335 and MAE. However, we used that model to make our temporal predictions because
 336 the MAE values are very similar among the considered models. Figure 9(a) shows
 337 the temporal predictions obtained for three of the nine rainfall stations, the temporal

338 areal prediction for the areal rainfall is presented in Figure 9(b), and the predicted
 339 series for runoff is displayed in Figure 9(c). Note that almost all of the true values
 340 are within the limits of the 95% posterior credible interval provided by our approach.



(a) Predicted rainfall at some stations (1,2,3 marked in Figure 1(a))



(b) Predicted rainfall for the basin

(c) Predicted runoff

Figure 9. Rainfall-Runoff forecast values. Mean (solid lines) and 95% credible interval (dashed lines) of predictive distributions. x : in (a) and (c) correspond to the observed data, in (b) corresponds to the values obtained with the Thiessen method.

341 6 Concluding remarks

342 In this paper we proposed a joint model for rainfall and runoff, by taking into account
 343 all the uncertainty associated with both stochastic processes and considering their
 344 different spatial units. We used some previously established individual models whose
 345 parameters have natural physical interpretations. We also fitted the data in their

346 original scale. Under a Bayesian framework we proposed to fit non-normal (gamma)
347 transfer function models using the CUBS sampling scheme that significantly re-
348 duces the computational time and is easy to implement. We were also careful with
349 the implementation of the MCMC algorithm. Although it is not shown here, missing
350 data are naturally handled as parameters of the models. We believe our approach is
351 a promising tool for runoff-rainfall analysis.

352 A natural extension of the model proposed here is the inclusion of a variable that
353 represents the region's vegetation. Vegetation controls the evapotranspiration and
354 interception processes, two components of the water balance.

355 Natural alternatives to the models used here are to consider other transfer func-
356 tions for the runoff and to consider other spatial correlation functions in the spatio-
357 temporal model for rainfall. An interesting extension is the use of hierarchical dy-
358 namic models (like [Gamerman & Migon \(1993\)](#)), to model a set of runoff series
359 from different basins but with similar geological and climate characteristics. Also,
360 linear models can be considered for both parameters of the biparametric gamma
361 distribution used for runoff, as in [Capkun et al. \(2001\)](#).

362 Finally, the results obtained with our approach provide an important input to the
363 decision problem of reservoir operations (see [Rios-Insua et al. \(1997\)](#)), which is just
364 one of the topics of our current research.

365 **Acknowledgments**

366 The work of Romy R. Ravines was supported by *Coordenação de Aperfeiçoamento*
367 *de Pessoal de Ensino Superior* (CAPES-Brazil). Alexandra M. Schmidt and Helio
368 S. Migon were supported by *Conselho Nacional de Desenvolvimento Científico e*
369 *Tecnológico* (CNPq-Brazil). The authors thank the *Laboratório de Hidrologia* of the
370 *Universidade Federal do Rio de Janeiro* (UFRJ), Brazil for providing the Rio Grande
371 basin data.

372 **References**

- 373 CAPKUN, G., DAVISON, A. C. & MUSY, A. (2001). A robust rainfall-runoff transfer
374 model. *Water Resources Research* 37 3207–3216.
- 375 CRESSIE, N. (1993). *Statistics for Spatial Data*. New York: Wiley & sons.
- 376 DOORNIK, J. (2002). *Object-Oriented Matrix Programming Using Ox*. London:
377 Timberlake Consultants Press and Oxford, 3rd ed. URL [www.nuff.ox.ac.uk/](http://www.nuff.ox.ac.uk/Users/Doornik)
378 [Users/Doornik](http://www.nuff.ox.ac.uk/Users/Doornik).
- 379 FERNANDES, M. V., SCHMIDT, A. M. & MIGON, H. S. (2007). Modelling
380 zero-inflated spatio-temporal processes. Technical report, no. 194/2006, De-
381 partamento de Métodos Estatísticos, Universidade Federal do Rio de Janeiro.
382 (<http://dme.ufrj.br/alex/FernandesSchmidtMigon.pdf>).
- 383 FRÜHWIRTH-SCHNATER, S. (1994). Data augmentation and dynamic linear models.
384 *Journal of Time Series Analysis* 15 183–202.

- 385 GAMERMAN, D. & LOPES, H. F. (2006). *Markov Chain Monte Carlo: Stochastic*
386 *Simulation for Bayesian Inference*. New York: Chapman & Hall / CRC.
- 387 GAMERMAN, D. & MIGON, H. (1993). Dynamic hierarquical models. *Journal of*
388 *the Royal Statistical Society, B* 85 629–642.
- 389 GELFAND, A. E. & GHOSH, S. (1998). Model choice: a minimum posterior predic-
390 tive loss approach. *Biometrika* 85 1–11.
- 391 GELFAND, A. E. & SMITH, A. (1990). Sampling-based approaches to calculating
392 marginal densities. *Journal of the American Statistical Association* 85 398–409.
- 393 GELFAND, A. E., ZHU, L. & CARLIN, B. (2001). On the change of support problem
394 for spatio-temporal data. *Biostatistics* 2 31–45.
- 395 GELMAN, A. & RUBIN, D. (1992). Inference from iterative simulation using multiple
396 sequences. *Statistical Science* 7 457–511.
- 397 LU, Z.-Q. & BERLINER, L. M. (1999). Markov switching time series models with
398 application to a daily runoff series. *Water Resources Research* 35 523–534.
- 399 MIGON, H. & MONTEIRO, A. B. (1997). Rain-fall modelling: An application of
400 Bayesian forecasting. *Stochastic Hydrology and Hydraulics* 11 115–127.
- 401 NEAL, R. (2003). Slice sampling (*with discussion*). *Annals of Statistics* 31 705–767.
- 402 PLUMMER, M., BEST, N., COWLES, K. & VINES, K. (2005). *CODA: Output*
403 *analysis and diagnostics for MCMC*. R package version 0.9-5, URL [http://](http://www-fis.iarc.fr/coda/)
404 www-fis.iarc.fr/coda/.
- 405 RAVINES, R., MIGON, H. S. & SCHMIDT, A. M. (2007). An efficient sam-
406 pling scheme for generalized dynamic models. Technical report, Departamento

- 407 de Métodos Estatísticos, Universidade Federal do Rio de Janeiro.
- 408 RIOS-INSUA, D., MONTES, R. & PALOMO, J. (2002). Bayesian methods in hydrology: a review. *Revista de la Real Academia de Ciencias. Serie A. Matemática* 96
409 461–479.
- 411 RIOS-INSUA, D., SALEWIZ, K., MÜLLER, P. & BIELZA, C. (1997). Bayesian
412 methods in reservoir operations: the Zambezi river case. In S. French & J. Smith,
413 eds., *The practice of Bayesian Analysis*. Arnold, 107–130.
- 414 SALES, P. (1989). *Procedimentos lineares para identificação e estimação de*
415 *parâmetros de modelos para séries temporais uni e multivariadas*. Ph.D. thesis,
416 Engenharia de Produção, COPPE - UFRJ, Rio de Janeiro, Brazil. (in Portuguese).
- 417 SANSÓ, B. & GUENNI, L. (2000). A non-stationary multi-site model for rainfall.
418 *Journal of the American Statistical Association* 95 1089–1100.
- 419 SCHMIDT, A. M. & GELFAND, A. E. (2003). A Bayesian coregionalization approach
420 for multivariate pollutant data. *Journal of Geophysical Research-Atmospheres*
421 108, No. D24, 8783.
- 422 SPIEGELHALTER, D., BEST, N., CARLIN, B. & DER LINDE, A. V. (2001). Bayesian
423 measures of model complexity and fit. *Journal of the Royal Statistical Society, B*
424 64 583–639.
- 425 VELARDE, L., MIGON, H. & PEREIRA, B. (2004). Space time modeling of non-
426 negative variables with point of mass at zero. *Environmetrics* 15 561–576.
- 427 WEST, M. & HARRISON, J. (1997). *Bayesian Forecasting and Dynamic Models*.
428 New York: Springer-Verlag, 2nd ed.
- 429 WEST, M., HARRISON, J. & MIGON, H. (1985). Dynamic generalized linear models

430 and Bayesian forecasting. *Journal of the American Statistical Association* 80 73–
 431 83.

432 A Likelihood and Spatial Change of Support

Here we present in more detail the computations for the change of support problem. Let $\mathbf{Y} = (Y_1, \dots, Y_T)'$, $\mathbf{X} = (X_1, \dots, X_T)'$, and $\mathbf{X}(s_i) = (X_1(s_i), \dots, X_T(s_i))'$. Also, consider $\mathbf{X}_t(\mathbf{s}) = (X_t(s_1), \dots, X_t(s_S))'$ and $\mathbf{X}(\mathbf{s}) = (\mathbf{X}_1(\mathbf{s}), \dots, \mathbf{X}_T(\mathbf{s}))$ an $S \times T$ matrix, where $\mathbf{s} = (s_1, \dots, s_S)$. The joint distribution of \mathbf{Y} and $\mathbf{X}(\mathbf{s})$ is given by

$$\begin{aligned} \underbrace{p(\mathbf{Y}, \mathbf{X}(\mathbf{s})|\Theta)}_{\text{observed data}} &= \int p(\mathbf{Y}, \mathbf{X}|\mathbf{X}(\mathbf{s}), \Theta) p(\mathbf{X}(\mathbf{s})|\Theta) \underbrace{d\mathbf{X}}_{\text{latent process}} & (A.1) \\ &= \int p(\mathbf{Y}|\mathbf{X}, \mathbf{X}(\mathbf{s}), \Theta_Y) \underbrace{p(\mathbf{X}, \mathbf{X}(\mathbf{s})|\Theta_X)}_{\text{Monte Carlo approximation}} d\mathbf{X}, \end{aligned}$$

433 where $\Theta = (\Theta_Y, \Theta_X)$. Actually, the joint distribution of the observed data is
 434 given by $p(\mathbf{Y}, \mathbf{X}(\mathbf{s})|\Theta)$, then \mathbf{X} plays the role of a latent variable. Since one of the
 435 advantages of the use of MCMC methods is that we can sample $p(\mathbf{Y}, \mathbf{X}, \mathbf{X}(\mathbf{s})|\Theta)$
 436 and consider that samples from $p(\mathbf{Y}, \mathbf{X}(\mathbf{s}))$ belong to the marginal joint distribution
 437 of both variables, we are concerned with $p(\mathbf{Y}, \mathbf{X}, \mathbf{X}(\mathbf{s})|\Theta)$, which for a fixed t is
 438 given by

$$p(Y_t, X_t, \mathbf{X}_t(\mathbf{s})|\Theta) = p(Y_t|X_t, \mathbf{X}_t(\mathbf{s}), \Theta_Y) p(X_t, \mathbf{X}_t(\mathbf{s})|\Theta_X). \quad (A.2)$$

Now, we focus on $p(X_t, \mathbf{X}_t(\mathbf{s})|\Theta_X)$. Recall that

$$X_t = \int_B \mathbf{X}_t(\mathbf{s}) d\mathbf{s}, \quad (A.3)$$

that is, X_t is a “function” of $\mathbf{X}_t(\mathbf{s})$ and the predictive distribution of X_t is

$$\underbrace{p(X_t|\mathbf{X}_t(\mathbf{s}))}_{\text{predictive}} = \int p(X_t|\mathbf{X}_t(\mathbf{s}), \boldsymbol{\Theta}_X) \underbrace{p(\boldsymbol{\Theta}_X|\mathbf{X}_t(\mathbf{s}))}_{\text{posterior}} d\boldsymbol{\Theta}_X. \quad (\text{A.4})$$

The moments of $p(X_t|\mathbf{X}_t(\mathbf{s}))$ in (A.4) involve integrals with respect to \mathbf{s} . For instance, assuming that the joint distribution of X_t and $\mathbf{X}_t(\mathbf{s})$ is normal, we have

$$E(X_t|\boldsymbol{\Theta}_X) = \int_B E(\mathbf{X}_t(\mathbf{s})|\boldsymbol{\Theta}_X) d\mathbf{s}. \quad (\text{A.5})$$

Gelfand et al. (2001) proposed to approximate those moments by means of Monte Carlo integration. They showed that

$$\hat{p}((X_t, \mathbf{X}_t(\mathbf{s}))'|\boldsymbol{\Theta}_X) = p((\hat{X}_t, \mathbf{X}_t(\mathbf{s}))'|\boldsymbol{\Theta}_X), \quad (\text{A.6})$$

where $\hat{\cdot}$ denotes a Monte Carlo integration and

$$\hat{X}_t = \sum_{i=1}^{S_B} \hat{X}_t(s_i) \quad i = 1, \dots, S_B. \quad (\text{A.7})$$

439 According to Gelfand et al. (2001), (A.6) implies that the approximated joint density
 440 of X_t and $\mathbf{X}_t(\mathbf{s})$ is equal to the joint density of \hat{X}_t and $\mathbf{X}_t(\mathbf{s})$, so, in practice, \hat{X}_t is
 441 the one to be sampled. The authors stated that $\hat{X}_t \rightarrow^P X_t$ if $\mathbf{X}_t(\mathbf{s})$ is almost surely
 442 a continuous process.